Chapter 6
Photon Interaction with Clusters and Microparticles

Abstract There are various mechanisms of particle interaction with photons that cause photon absorption. In the case of dielectric particles it results from interaction of the radiation field with a particle dipole moment which is induced by this field. Absorption of infrared radiation by a particle proceeds by excitation of internal degrees of freedom that in the case of separation of the particle in molecules corresponds to molecular vibrations and rotations. The latter is of importance for radiative transitions in aerosols, i.e. in atmospheric particles. The interaction of metal particles with an electromagnetic wave takes place through an electron subsystem twofold. If the electron subsystem partakes in this interaction as a whole, the photon absorption is determined by its plasma properties. In other case, the absorption results from electron excitation of metal atoms which constitute the metal particle. In particular, from the analysis of experimental data it is shown that light absorption is described by radiative transitions in individual atoms which interact strongly with surrounding ones. In addition, electrons of the metal particles screen an electromagnetic field, and if a particle size is not too small, absorption proceeds in a thin layer near its surface, or in the skin layer.

6.1 Scattering of the Electromagnetic Wave on Atomic and Small Particles

6.1.1 Resonance Fluorescence Involving Molecules and Atoms

Interaction of an atomic particle with an electromagnetic wave results in processes of scattering of this wave and its absorption. Elementary processes of photon collisions with a molecule are presented in Fig. 6.1. They include one-photon processes—absorption and emission during photon-molecule collisions. Last three processes are two-photon processes. Rayleigh scattering is an elastic photon-molecule process,

V. Krainov and B. M. Smirnov, *Atomic and Molecular Radiative Processes*,
Springer Series on Atomic, Optical, and Plasma Physics 108,
https://doi.org/10.1007/978-3-030-21955-0_6

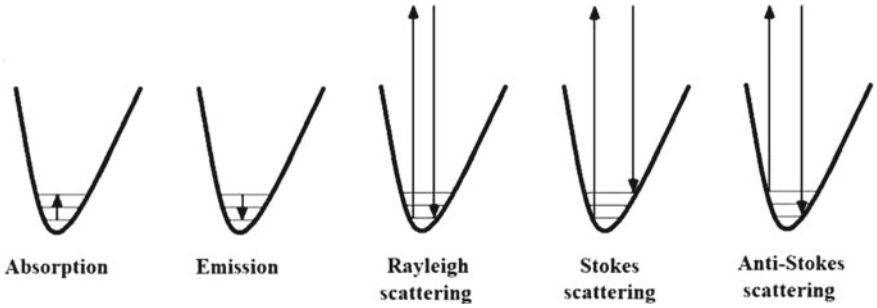

Fig. 6.1 Types of photon scattering on the molecule

other two processes in Fig. 6.1, i.e. the Stokes process and anti-Stokes process, are inelastic collisions with a loss and increase of the photon energy.

One can see the symmetry between some processes of Fig. 6.1. This symmetry is expressed through the principle of detailed balance which connects the cross sections of direct and inverse processes with each other. In particular, the symmetry between one-photon processes, i.e. between processes of emission and absorption, follows from formulas (2.2.24) and (2.2.25). We below show the connection between the Stokes process and anti-Stokes one, i.e. two-photon processes in photon-molecule scattering which are presented in Fig. 6.1.

Note that the most intense Stokes and anti-Stokes processes as a result of two-photon scattering on a molecule are realized, if the first step of these processes is the resonance photon absorption in accordance with Fig. 6.2 for molecule transitions. Similar resonance processes for atoms are shown in Fig. 6.3; they take into account that the final state include a group of levels which may be degenerated. These levels belong to states of fine or superfine structures; we characterize each level by a momentum J_0 for the initial state and a momentum J_k for the final state, so that the statistical weights for the initial state g_0 and for the final one are

$$g_0 = 2J_0 + 1, \;\; g_k = 2J_k + 1$$

We below determine the connection between rates of the processes of resonance fluorescence which are shown in Fig. 6.3. These processes are detailed inverse ones, and we use the cross section of photon absorption (2.2.24) for the total radiative process as a transition between electron terms, and the radiative time τ_{k0} accounts for the radiative transition between electron terms which are identical for both radiative processes in Fig. 6.3. In considering the transition states i and j of these processes as to be related to the same electron state and assuming the process to be incoherent, one can express the cross sections of the processes of Fig. 6.3 through the same parameters. Indeed, assuming the collision character of broadening of spectral lines, we have for the cross section of the direct radiative process using the formula (2.2.24)

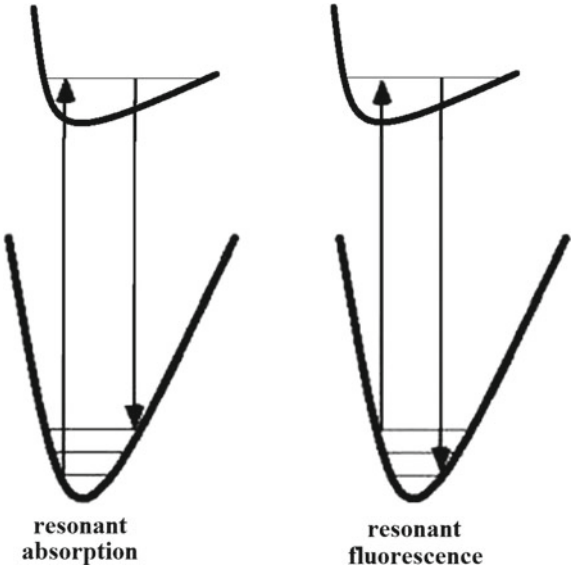

Fig. 6.2 Resonant photon scattering on a molecule, so that the first step of the radiative process is photon absorption, and the second step is photon emission

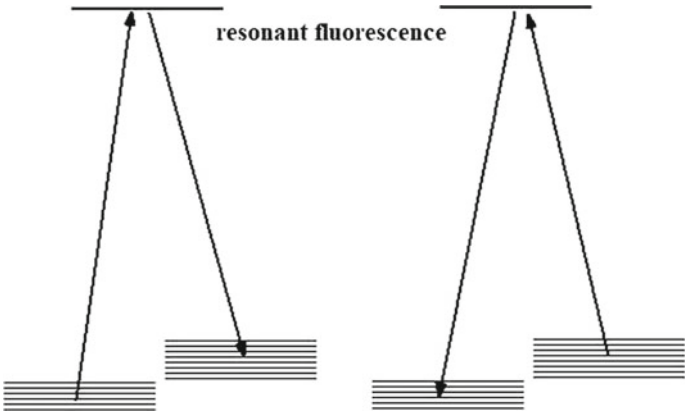

Fig. 6.3 Resonance fluorescence in photon scattering on an atom; the initial and final states include the corresponding group of levels

$$\sigma(\omega,\ i \to j) = \frac{2J_k + 1}{2(2J_0 + 1)} \frac{\pi c^2}{\omega^2} \frac{1}{\tau_{mi}\tau_{jm}} \frac{1}{\left[(\omega_{ji} - \omega)^2 + (\nu/2)^2\right]}, \tag{6.1.1}$$

where $\omega_{ji} = (E_j - E_i)/h$, so that E_j, E_i are the energies of these levels, m is an intermediate state, τ_{mi}, τ_{jm} are partial radiative lifetimes of an intermediate state m with respect to the transition into states i and j respectively. In the same manner we

have for the cross section of the inverse process

$$\sigma(\omega,\ j \to i) = \frac{2J_0 + 1}{2(2J_k + 1)} \frac{\pi c^2}{\omega^2} \frac{1}{\tau_{mi}\tau_{jm}} \frac{1}{\left[(\omega_{ji} - \omega)^2 + (\nu/2)^2\right]}, \tag{6.1.2}$$

It should be noted that if we assume the radiation to be incoherent and therefore it is based on statistical principles, one can obtain the probability of the transition to a state of this group of levels as $1/2J + 1$. If the width of the spectral line is determined by radiative decay of the excited state, one can obtain an estimate for the fluorescence cross section $\nu \sim 1/\tau mi$

$$\sigma \sim \frac{\pi c^2}{\omega^2} \sim \pi\bar{\lambda}^2, \tag{6.1.3}$$

where $\bar{\lambda} = c/\omega$ is the photon wavelength. It is seen that this cross section does not depend on the fine structure constant $\alpha = e^2/\hbar c$ unlike the analogous non-resonance cross sections. Hence, the cross section for resonance fluorescence is much larger (in $(\omega_{ji}\tau_{ji})^2$ times) than the cross section for non-resonance fluorescence. Note also that (6.1.3) is the maximum cross section of photon absorption, for the transition of the atomic particle from the state i to the state j.

6.1.2 Raman Scattering on Atomic Particles

Raman spectroscopy is based on the elastic light scattering (see Fig. 6.1) that gives information about molecular vibrations. In the case of the Rayleigh scattering the energy exchange between incident and scattered photons is absent. But due to the interaction with the molecule, a photon can obtain vibrational quanta from the molecule, and then this process is known as anti-Stokes Raman scattering. Oppositely, if the molecule acquires vibration quanta from the photon, then the frequency of scattered light is lower than that of the incident light, and this process is called Stokes Raman scattering.

Combination scattering (or Raman scattering) [1–6] is photon scattering on atomic particles or on atomic systems at which the direction of the photon motion and, possibly, its frequency, change (Fig. 6.1). We consider here only relatively weak intensities of the electromagnetic wave, when the radiation electric field strength is assumed to be small compared to the atomic field strength. Then the process of the radiation scattering on atomic particles (or systems) is a two-photon process; various channels of this process are shown in Fig. 6.1. Participation of three and more photons is insignificant due to the weak radiation intensity. It is seen from Fig. 6.1 that there are three channels of the photon scattering during its capture by a virtual level and subsequent birth of another photon. In the case of the Rayleigh scattering the photon with the same frequency appears, while at the Stokes and anti-Stokes scattering

processes, the atomic particle transfers to higher, or lower level, respectively. In the case of photon scattering on molecules, the Stokes and anti-Stokes processes allows to determine the molecular spectrum for a given symmetry of states.

We here regard photon scattering as a two-photon process in which the first photon of frequency ω_1 is absorbed and a second photon of frequency ω_0 is emitted, with the simultaneous transition of an atomic electron from the initial state i to the final state j. This process differs from fluorescence in that the final state j can differ from the initial state i (this is so-called combination scattering or Raman scattering). Consider first the case of resonant Raman scattering, where the photon frequency ω_1 is nearly the same as the excitation frequency ω_{ji} of the state i of the atomic electron. The photo-absorption distribution function is given by (2.1.40). Subsequent steps in the solution of this problem are parallel to the solution in Sect. 2.1, except that (2.1.40) should be multiplied by the factor τ_j/τ_{mj}, where τ_{mj} is the lifetime of the state m with respect to the transition into the final state j. As a result, instead of (2.1.40) we find

$$\sigma_c = \frac{2J_k+1}{2\,(2J_0+1)}\,\frac{\pi c^2}{\omega^2}\,\frac{1}{\tau_{mj}\tau_{mi}}\,\frac{1}{(\omega_{mi}-\omega)^2+[1/\,(2\tau_m)]^2}. \tag{6.1.4}$$

In particular, the result at the exact resonance is

$$\sigma_c^{\max} = \frac{2J_k+1}{2\,(2J_0+1)}\,\frac{4\pi c^2}{\omega^2}\,\frac{\tau_k^2}{\tau_{jm}\tau_{mi}}. \tag{6.1.5}$$

As should be the case, this quantity is less than the maximum value for the photoabsorption cross section. We observe that (6.1.4) is of the same order of magnitude as the resonant fluorescence cross section.

We now treat nonresonance Raman scattering. The probability of the two-photon transition induced by fields with electric field strengths E_1 and E_2 is determined by the second-order perturbation theory. According to the "Fermi golden rule" of quantum mechanics we have

$$w_{ij} = \frac{\pi E_1^2 E_2^2}{8\hbar^2}\left|\sum_m\left[\frac{(\mathbf{s}_2\mathbf{D}_{jm})\,(\mathbf{s}_1\mathbf{D}_{mi})}{\omega_{ji}-\omega_1}+\frac{(\mathbf{s}_1\mathbf{D}_{jm})\,(\mathbf{s}_2\mathbf{D}_{ji})}{\omega_{mi}+\omega_2}\right]\right|^2\delta\left(\omega_{ji}-\omega_1+\omega_2\right) \tag{6.1.6}$$

Here we take into account that the incident photon with the frequency ω_1 is absorbed, and the photon with the frequency ω_2 is emitted.

According to results of the Chap. 1 we can connect the electric field strength E of the incident electromagnetic wave with the photon number n_ω

$$E^2 = \frac{8\hbar\omega^3\delta\omega}{\pi c^3}n_\omega$$

($\delta\omega$ is the difference of frequencies of the neighboring modes). Then, substituting

$$\sum_k \to \frac{1}{\delta\omega}\int \mathrm{d}\omega, \tag{6.1.7}$$

in (6.1.2), one obtains

$$w_{0m} = \left|\sum_k \left[\frac{(\mathbf{s}_2\mathbf{D}_{mk})\,(\mathbf{s}_1\mathbf{D}_{k0})}{\omega_{k0}-\omega_1} + \frac{(\mathbf{s}_1\mathbf{D}_{mk})\,(\mathbf{s}_2\mathbf{D}_{k0})}{\omega_{k0}+\omega_2}\right]\right|^2 \delta\left(\omega_{m0}-\omega_1+\omega_2\right)\times$$
$$\times\,\frac{\omega_1\omega_2 d\mathbf{k}_1 d\mathbf{k}_2}{8\pi^3\hbar^2}. \tag{6.1.8}$$

Here we suppose that in the incident photon beam there are no photons with the frequency ω_2, that is $n_{\omega_2}=0$.

Since both absorbed and emitted photons in (6.1.8) have definite polarizations (s_1 and s_2, accordingly), then the flow density of incident photons is equal to

$$j_\omega = \frac{n_{\omega_1}\omega_1^2 \mathrm{d}\omega_1}{2\pi^2 c^3} \tag{6.1.9}$$

Thus it follows from (6.1.8) the expression for cross section of nonresonance combination scattering

$$d\sigma_c = \frac{\omega_1\omega_2^3}{c^4\hbar^2}\left|\sum_m \left[\frac{(\mathbf{s}_2\mathbf{D}_{mk})\,(\mathbf{s}_1\mathbf{D}_{mi})}{\omega_{mi}-\omega_1} + \frac{(\mathbf{s}_1\mathbf{D}_{mk})\,(\mathbf{s}_2\mathbf{D}_{mi})}{\omega_{mi}+\omega_2}\right]\right|^2 \mathrm{d}\Omega_2. \tag{6.1.10}$$

In the derivation of this expression we integrated (6.1.8) over frequency ω_2 of the emitted photon, using the energy conservation law for this process. The quantity $\mathrm{d}\Omega_2$ is the solid angle of the scattered photon, and m is the index labeling the final state of the atomic electron. The energy conservation law gives $\omega_{ji}-\omega_1+\omega_2=0$. In particular, when the initial and final states are the same, that is, when $j=i$ and $\omega_1=\omega_2$, (6.1.10) gives the nonresonance fluorescence cross section.

Now we calculate the cross section for photon scattering by a free electron. We suppose that the energy of the incident photon is small as compared to the electron rest energy, that is, $\hbar\omega \ll m_\mathrm{e}c^2$. The photon momentum is $\hbar\omega/c$. The change of photon momentum in the scattering process and the electron momentum after scattering are of the same order of magnitude: $\hbar\omega/c$ (excluding scattering through very small angles). The energy gained by the electron in the collision is of the order of $(\hbar\omega)^2/\left(m_\mathrm{e}c^2\right)$; it is small as compared to the rest energy, which is equivalent to the statement that the velocity increment v of the electron from the scattering is small as compared to c. The electron motion is thus nonrelativistic one. Since the change of the energy of the photon, also $\sim(\hbar\omega)^2/\left(mc^2\right)$, is small compared to the initial photon energy $\hbar\omega$, the photon-electron scattering is quasi-elastic, which means $\omega_1 \cong \omega_2$.

We shall use (6.1.10) for the calculation of the cross section assuming that $\omega_1=\omega_2$, and using the semiclassical approximation for the free electron states due to the

semiclassical character of the initial continuum electron state i. The dipole operator of an electron is $D = -er$, where r is the electron coordinate. Equation (6.1.4) leads to

$$\mathrm{d}\sigma_c = \frac{4\omega^4}{c^4\hbar^2}\left|\sum_m (\mathbf{s}_2\mathbf{r}_{im})\,(\mathbf{s}_1\mathbf{r}_{mi})\,\frac{\omega_{mi}}{\omega_{mi}^2-\omega^2}\right|^2 \mathrm{d}\Omega. \tag{6.1.11}$$

We wish to evaluate the sum in (6.1.11). The coordinate axes are selected so that s_1 is along the z axis and s_2 is in the xz plane. The sum is then of the form

$$s_{2x}\sum_k \omega_{mi}x_{im}z_{k0} + s_{2z}\sum_m \omega_{mi}\,|z_{mi}|^2\,.$$

The first of the sums in this expression is zero because of the odd parity of the product $\omega_{mi}x_{im}z_{mi}$: it changes sign when $z \to -z$. The second sum can be calculated using the sum rule, (1.3.20) of the Sect. 1.3.2, for dipole transitions. The above expression then yields

$$\frac{\hbar s_{2z}}{2m_e} = \frac{\hbar\,(\mathbf{s}_1\mathbf{s}_2)}{2m_e} \tag{6.1.12}$$

Substituting this expression into (6.1.11) for cross section of Raman scattering gives this cross section in the form

$$\mathrm{d}\sigma = r_e^2\,(\mathbf{s}_1\mathbf{s}_2)^2\,\mathrm{d}\Omega \tag{6.1.13}$$

Here the quantity

$$r_e = \frac{e^2}{m_e c^2} \tag{6.1.14}$$

is the classical electron radius. Equation (6.1.13) is called the Thomson formula. It is a purely classical result, since the Planck constant does not appear. To calculate the total cross section, we integrate (6.1.13) over the solid angle $\mathrm{d}\Omega$. We select the polar axis of a system of spherical coordinates to lie along the polarization vector s_1 of the incident photon. The notation θ is introduced for the angle between vectors s_1 and k_2. Since vectors s_2 and k_2 are perpendicular to each other, then we find that $s_1 s_2 = \sin\theta$. If the vector s_2 is normal to the plane composed from vectors s_1 and k_2 the cross section of scattering is zero, since then vectors s_1 and s_2 will be normal to each other. Hence,

$$\sigma = r_e^2\int \sin^2\theta \mathrm{d}\Omega = \frac{8\pi}{3}r_e^2. \tag{6.1.15}$$

Equations (6.1.13) and (6.1.15) can be also obtained in the classical radiation theory by solving the Newtonian equations of motion for induced electron oscillations and considering the emission of secondary waves with the same frequency. The classical results fail when the photon energy $\hbar\omega$ is of the order of the electron rest energy mc^2 or greater. Then most of the incident photon energy is transferred to

the electron, and the scattering is therefore inelastic. In this case, relativistic and quantum effects will be important simultaneously, and the electron spin will be also an essential element in the description of the scattering.

Further we calculate the low-energy scattering cross section for a photon scattering from an atom with zero angular momentum. The frequency of the photon is taken to be small compared to typical atomic frequencies, $\omega \ll \omega_{mi}$. This limit is thus opposite to that considered for a photon scattering of a free electron with $\omega \gg \omega_{mi}$. The small frequency condition allows us to simplify (6.1.10) to

$$\mathrm{d}\sigma_c = \frac{4\omega^4}{c^4\hbar^2}\left|\sum_m \frac{(\mathbf{s}_2\mathbf{D}_{im})\,(\mathbf{s}_1\mathbf{D}_{mi})}{\omega_{mi}}\right|^2 \mathrm{d}\Omega, \tag{6.1.16}$$

The initial state i is specified to be an S state, so that its magnetic quantum number is $M_i = 0$. The state m is therefore a P state in accordance with the dipole selection rule, and so $M_m = 0, \pm 1$. We take the axis of quantization z to lie along s_1. The vector D is along the z direction. In the opposite case, the quantity $D_{im}s_1$ vanishes. Hence we have

$$\mathbf{D}_{0k}\mathbf{s}_2 = (\mathbf{s}_1\mathbf{s}_2)\,(D_z)_{im}\,. \tag{6.1.17}$$

We now define the polarizability tensor

$$\alpha_{ij} = 2\sum_m \frac{(D_i)_{im}\left(D_j\right)_{mi}}{\hbar\omega_{mi}} \tag{6.1.18}$$

It follows from the above considerations that α_{ij} is a diagonal tensor, so that $\alpha_{ij} = \alpha\delta_{ij}$ and

$$\alpha = \frac{2e^2}{\hbar}\sum_m \frac{|z_{mi}|^2}{\omega_{mi}}. \tag{6.1.19}$$

When this result is substituted into (6.1.16), we find the scattering cross section

$$\mathrm{d}\sigma = \frac{\omega^4\alpha^2}{c^4}\,(\mathbf{s}_1\mathbf{s}_2)^2\,\mathrm{d}\Omega = \frac{\omega^4\alpha^2}{c^4}\,\sin^2\theta\mathrm{d}\Omega, \tag{6.1.20}$$

where θ is the angle between the polarization direction s_1 of the incident photon and the direction k_2 of the wave vector of the scattered photon. After integration over the angular coordinates, we find the total cross section for photon scattering by an atom in the low photon frequency limit to be

$$\sigma = \frac{8\pi\omega^4\alpha^2}{3c^4}. \tag{6.1.21}$$

We now wish to solve the same problem by the classical approach. From (1.2.31), the intensity of scattered light is

$$I(t) = \frac{2}{3c^3}\left|\ddot{\mathbf{D}}(t)\right|^2, \tag{6.1.22}$$

where $\mathbf{D}$ is the induced dipole moment produced by the field of an electromagnetic wave with an electric field given by $\mathbf{E}\cos\omega t$. By the definition of atomic polarizability α, we have $\mathbf{D} = -\alpha\mathbf{E}\cos\omega t$. We are thus led to the intensity of scattered light expressed as

$$I(t) = \frac{2\omega^4\alpha^2}{3c^3}\mathbf{E}^2\cos^2\omega t. \tag{6.1.23}$$

To find the cross section, we should divide this quantity by the energy flux of the incident radiation. This energy flux is given by the Poynting vector $c\,[\mathbf{E}, \mathbf{H}]/4\pi$, where E and H are the electric and magnetic fields of the electromagnetic wave. In our case, the energy flux has the magnitude $cE^2\cos^2\omega t/4\pi$. When we define the scattering cross section as the ratio of the intensity of scattered light to the energy flux of the incident radiation, we obtain

$$\sigma = \frac{8\pi\omega^4\alpha^2}{3c^4}. \tag{6.1.24}$$

This agrees with the quantum result in (6.1.21). The advantage of the quantum-mechanical derivation is that it makes it possible to obtain the explicit expression for atomic polarizability. It is seen from the derivation that the scattering process considered is purely classical one. A classical dipole moment radiates the same frequency that is induced by the electromagnetic wave. Such scattering is called Rayleigh scattering. It is interesting that both Rayleigh scattering ($\omega \ll \omega_{ji}$) and Thomson scattering ($\omega \ll \omega_{ji}$) are purely classical phenomena. The maximum in the scattering of visible light by atoms with absorption frequencies in the ultraviolet range corresponds to the violet cut-off of the spectrum, since the scattering cross section increases very strongly with frequency: as ω^4. The limit $\omega \ll \omega_{ji}$ holds true nevertheless. This explains the blue color of the sky. Sunset is of a red color for the same reason: the strong scattering of the violet part of the solar spectrum in the direct flux of the solar rays leaves a predominance of red in the remaining part of the sunlight.

The static polarizability can be exactly calculated for the ground state of the hydrogen atom. The result is that $\alpha = (9/2)\,a_o^3$ where $a_o = \hbar^2/m_e e^2$ is the Bohr radius. Hence the cross section for the hydrogen ground state for low-energy photon scattering, with $\hbar\omega \ll \hbar^2/m_e a_o^2$, is given by

$$\mathrm{d}\sigma = \frac{81}{4}r_e^2\left(\frac{\hbar^3\omega}{me^4}\right)^4(\mathbf{s}_1\mathbf{s}_2)^2\mathrm{d}\Omega \tag{6.1.25}$$

This expression describes accurately the elastic scattering cross section from zero frequency up to the frequency of the first resonance when $\hbar\omega = \hbar\omega_{k0} = 3me^4/\left(8\hbar^2\right)$. The indices 1 and 2 refer, respectively, to the ground and first excited states of the

hydrogen atom. An additional problem with accounting for degeneracy of the state i with respect to magnetic quantum numbers appears in the case of nonzero angular momentum. If the low-energy photon is scattered by an atom in an excited state, then Raman scattering occurs as well as Rayleigh scattering, with the consequent transition of the atom to a lower lying state m.

We now calculate the dependence of the intensity of induced Raman scattering on the propagation distance of the photon beam in the gas. We consider (6.1.10) for the Raman scattering cross section $d\sigma_c$ when an atomic electron makes a transition from the initial state i to the final state j. If we denote by N/Ω the density of atoms, then the quantity

$$g = \frac{N}{\Omega}\sigma_c \tag{6.1.26}$$

presents the number of photons with frequency ω_2 that is generated in a unit distance along the photon beam. The total Raman scattering cross section, σ_c, is obtained from (6.1.10) by performing the integration over the angles of the emitted photons of frequency ω_2.

We now have $n_{\omega_2} \neq 0$, since the photons transfer from an incident beam of frequency ω_1 to photons of scattered light with frequency ω_2. If we select coordinates with the z axis along the propagation direction of the incident beam, then by the requirement that each absorbed photon gives rise to a scattered photon, we have

$$n_{\omega_1}(z) + n_{\omega_2}(z) = \text{const} = n_{\omega_1}(0), \tag{6.1.27}$$

where $n_{\omega_1}(0)$ is the initial amount of photons in the incident beam. In the usual scheme of quantization, each mode of oscillation is contained in the volume Ω, so we suppose that the typical characteristic length along the z axis is much greater than $\Omega^{1/3}$. We can now write balance equations that determine the dependence of the quantities $n_{\omega_1}(z)$ and $n_{\omega_2}(z)$ on z. Equation (6.1.26) establishes the amount of photons that appears in a unit length along the photon beam, under the condition that there is one photon of frequency ω_1 and no photons of frequency ω_2. However, if at the coordinate z we have the amount $n_{\omega_1}(z)$ photons with frequency ω_1 and $n_{\omega_2}(z)$ photons of frequency ω_2 then (6.1.8) means that the amount of photons appearing in a unit length along the beam with frequency ω_2 is

$$w(z) = g n_{\omega_1}(z)\left[1 + n_{\omega_2}(z)\right]. \tag{6.1.28}$$

Hence, the balance equations are of the simple form

$$\frac{\mathrm{d}n_{\omega_1}(z)}{\mathrm{d}z} = -\frac{\mathrm{d}n_{\omega_2}(z)}{\mathrm{d}z} = -w(z). \tag{6.1.29}$$

The solution of the system (6.1.29) under the conditions (6.1.27) is elementary. We write it in the form

$$n_{\omega_2}(z) = \frac{\exp(Gz) - 1}{1 + \left[\exp(Gz)/n_{\omega_1}(0)\right]}, \tag{6.1.30}$$

where the quantity G is defined as

$$G = g\left[1 + n_{\omega_1}(0)\right] = \frac{N}{\Omega}\sigma_c\left[1 + n_{\omega_1}(0)\right]. \tag{6.1.31}$$

The quantity G is called the *increment coefficient*. We see that the amount of scattered photons increases at first linearly with z. This corresponds to the general theory developed above in this chapter. This linear dependence occurs when $Gz \ll 1$. When $Gz \sim 1$, the linear increase becomes an exponential one. Finally, when $Gz > 1$, saturation takes place, $n_{\omega_2}(z) \to n_{\omega_1}(0)$, so that all photons from the incident beam are replaced by photons in the scattered state.

The intensity of the induced Raman scattering for photons with frequency ω_2 is given by

$$I_2(z) = c\hbar\omega_2 \frac{n_{\omega_2}(z)}{\Omega}, \tag{6.1.32}$$

where $n_{\omega_2}(z)$ is determined by (6.1.27). In the linear regime, (6.1.30) becomes

$$n_{\omega_2}(z) = Gz \frac{n_{\omega_1}(0)}{1 + n_{\omega_1}(0)}, \tag{6.1.33}$$

which is in good agreement with (6.1.10). If we take the volume Ω with the length z in the direction of the photon beam with frequency ω_1, where N the number of atoms in this volume, then the cross section of the volume Ω is Ω/z. We now calculate the energy flux through this volume for the photons of frequency ω_1, and obtain

$$I_1(z)\frac{\Omega}{z} = c\hbar\omega_1 \frac{n_{\omega_1}(z)}{\Omega}\frac{\Omega}{z} = -Gc\hbar\omega_1 \frac{n_{\omega_1}(0)}{1 + n_{\omega_1}(0)} + c\hbar\omega_1 \frac{n_{\omega_1}(0)}{z}. \tag{6.1.34}$$

Using (6.1.31) for the parameter G we rewrite the first term in (6.1.34) in the form

$$-\frac{N}{\Omega}\sigma_c c\hbar\omega_1 n_{\omega_1}(0) \tag{6.1.35}$$

To calculate the cross section we divide (6.1.35) by the particle density N/Ω and by the photon flux of the incident photons $c\hbar\omega_1 n_{\omega_1}(0)$. As should be expected, we obtain σ_c, the Raman scattering cross section given in (6.1.10). In the nonlinear regime, the increment coefficient G is more useful than the cross section σ_c.

6.1.3 Rayleigh Scattering by Dielectric Particles

Scattering and absorption of solar light by small dielectric dust particles is produced by their polarization in the external electric field. There is no skin-layer inside a dielectric particle, so that the external field penetrates through the whole particle. Besides of this, the magnetic component of scattering is small compared to the electric part, due to absence of the conduction currents.

There are condensation nuclei, tiny suspended particles, either solid or liquid, upon which water vapor condensation begins in the atmosphere. There are also much smaller nuclei in the atmosphere. The discovery that the air is full of tiny particles around which water droplets may condense to create clouds was made by Scottish physicist John Aitken (1839–1919). Much smaller particles are called Aitken nuclei. They ordinarily play no role in cloud formation because they do not induce condensation unless the air is highly supersaturated with water vapor. Most condensation nuclei are produced by wave action over the oceans and by natural and man-made fires over land. When mixed with the more hygroscopic material, dust and soil particles blown into the atmosphere also are sources of nuclei. Numerous measurements provide support for the hypothesis that layers of high concentrations of Aitken nuclei near the tops of marine clouds are due to photochemical nucleation. Chemical factors support the view that Aitken nuclei are dielectric particles of sizes in the range 0.01–0.1 μm. On average, their concentration varies from less than $10^3/\text{cm}^3$ over oceans to $10^6/\text{cm}^3$ in urban areas. It is tentatively concluded that Aitken particles in the troposphere account for most of the sulfate in the atmosphere.

We first consider scattering of light on the dielectric dust particles. The radius of this particle r_o is assumed to be small compared to the wavelength of the incident light $\lambda = 2\pi c/\omega$, that is

$$\frac{\lambda}{r_o} \sim \frac{c}{\omega r_0} \ll 1. \tag{6.1.36}$$

We assume also that the dielectric permittivity $\varepsilon(\omega)$ is not too large, i.e. the condition

$$1 < \sqrt{\varepsilon} \ll \frac{c}{\omega r_o} \tag{6.1.37}$$

is fulfilled. Then we can solve the static problem (the Laplace equation) both inside and outside of the particle. It should be noted that the inequality (6.1.37) is fulfilled well also for polar molecules for which the dielectric permittivity ε is near unit for light range of the electromagnetic frequencies. As a result, the temporal dependence of the electrostatic potential can be neglected everywhere.

The Laplace equation for the electrostatic potential φ inside and outside of the particle is of the form

$$\varphi(r,\theta) = Cr\cos\theta;\ r \le r_o;\ \varphi(r,\theta) = (-Er + \frac{D}{r^2})\cos\theta;\ r \ge r_o \tag{6.1.38}$$

Here $a \ll \lambda, \lambda_e$ is the radius of the dust particle, and λ is the wavelength of the incident light, $\lambda_e = \lambda/\sqrt{\varepsilon}$ is the wavelength inside the particle. The quantity $\mathbf{E} = \mathbf{E}_0 \exp(-i\omega t)$ is the electric field strength of the incident light wave.

Using the continuity condition of the potential on the surface of the particle (at $r = r_o$), one obtains the connection between coefficients C and D

$$C = -E + \frac{D}{r_o^3}. \tag{6.1.39}$$

The second equation for these coefficients follows from the continuity condition for the normal component of the electric displacement

$$-\varepsilon C = E + \frac{2D}{r_0^3} \tag{6.1.40}$$

Excluding the quantity D from two last equations, one finds the value of C

$$C = -\frac{3}{\varepsilon + 2}E. \tag{6.1.41}$$

Thus, the field strength of the uniform electric field inside the small dust particle is

$$\mathbf{E}_{\text{in}} = \frac{3}{\varepsilon + 2}\mathbf{E} \tag{6.1.42}$$

The electric polarization $\mathbf{P}_{\text{in}}$ (the dipole moment of the unit volume) is also uniform everywhere inside the particle; it is equal to

$$\mathbf{P}_{\text{in}} = \frac{\varepsilon - 1}{4\pi}\mathbf{E}_{\text{in}} = \frac{3}{4\pi}\left(\frac{\varepsilon - 1}{\varepsilon + 2}\right)\mathbf{E}, \tag{6.1.43}$$

and the dipole moment of the whole dust particle is

$$\mathbf{p} = \frac{4\pi a^3}{3}\mathbf{P}_{in} = \left(\frac{\varepsilon - 1}{\varepsilon + 2}\right)a^3\mathbf{E}. \tag{6.1.44}$$

This solution is equivalent to the well known expression for the static dipole moment of the dielectric ball in a constant electric field. The difference is only that (6.1.44) contains the dielectric permittivity $\varepsilon(\omega)$ which corresponds to the frequency of the visible light, instead of the static dielectric constant ε_{st}. In the case of polar dielectrics the quantity ε_{st} can be several decimal orders of magnitude larger than the dielectric permittivity $\varepsilon(\omega)$ in the light frequency range. Now we determine the differential cross section of scattering; it is obtained from (6.1.20) by substitution the polarizability which is equal to ratio of the dipole moment (6.1.44) by the electric field strength of the incident light wave:

$$\mathrm{d}\sigma_s = \left(\frac{\varepsilon - 1}{\varepsilon + 2}\right)^2 \frac{\omega^4 r_o^6}{c^4} \left(1 - \sin^2\vartheta \cos^2\varphi\right) \mathrm{d}\Omega. \tag{6.1.45}$$

In order to consider the non-polarized solar light, we should average $\mathrm{d}\sigma_s$ over the angle φ :

$$\langle \mathrm{d}\sigma_s \rangle = \left(\frac{\varepsilon - 1}{\varepsilon + 2}\right)^2 \frac{\omega^4 r_o^6}{c^4} \frac{1 + \cos^2\vartheta}{2} \mathrm{d}\Omega. \tag{6.1.46}$$

Integrating over the solid angle, one obtains the total cross section of the Rayleigh light scattering on a small spherical dust particle:

$$\langle \sigma_s \rangle = \frac{8\pi}{3} \left(\frac{\varepsilon - 1}{\varepsilon + 2}\right)^2 \frac{\omega^4 r_o^6}{c^4}. \tag{6.1.47}$$

This cross section is proportional to ω^4, and it is much less than the geometrical cross section of the dust particle πr_o^2, if $a \ll \lambda \sim c/\omega$. It should be noted that in the opposite limiting case $a \ll \lambda$, the cross section coincides the geometrical cross section both for dielectric and for metal dust particles.

The Rayleigh law (6.1.47) $\sim\omega^4$ explains the cyan color of the heaven at the scattering of solar light. The maximum of the Planck spectrum of solar light corresponds to the yellow color. The difference in the intensity of cyan and violet components of the Planck solar light is less than 20%. The visible cyan color of the heaven is explained by the human eye sensitivity. The cyan light is perceived by the eye better than the violet light, by more than one order of magnitude!

6.1.4 Small Dielectric Particles in Electromagnetic Field

Scattering of an electromagnet wave on a macroscopic particle is determined by electric properties of the particle; in other words, scattering results from reaction of a particle material to the radiation field. Note that the polarizability of a particle α characterizes the particle reaction of the action of the electric field. This quantity is introduced as a connection between the induced dipole moment $\mathbf{D}$ of the particle and the electric field strength $\mathbf{E}$ which creates this dipole moment, so that

$$\mathbf{D}(\omega) = \alpha(\omega)\mathbf{E}(\omega) \tag{6.1.48}$$

We first establish the connection between the absorption cross section by a particle with its polarizability. Indeed, the interaction potential between the particle and electric field is $V = -\mathbf{DE}$. From this we have for the power absorbed by the particle

$$P = -\left\langle \mathbf{E} \frac{\mathrm{d}\mathbf{D}}{\mathrm{d}t} \right\rangle,$$

where brackets mean the averaging over time. Taking the electric field strength of a monochromatic electromagnetic wave in the form

$$\mathbf{E} = \mathbf{E}_0 \exp(i\omega t) + \mathbf{E}_0^* \exp(-i\omega t),$$

where ω is the frequency of the electromagnetic wave, we obtain for the particle dipole moment induced by the electromagnetic wave as

$$\mathbf{D} = \alpha(\omega)\,\mathbf{E}_0 \exp(i\omega t) + \alpha^*(\omega)\,\mathbf{E}_0^* \exp(-i\omega t),$$

where $\alpha(\omega)$ is the particle polarizability.

From this it follows for the absorbed power

$$P = i\omega |E_0|^2 \left(\alpha^* - \alpha\right)$$

The flux density of the electromagnetic energy is

$$J = \frac{c|E_0|^2}{2\pi}$$

Then the absorption cross section σ_{abs} by the particle as the ratio of the absorbed power density to the flux of the electromagnetic energy is equal

$$\sigma_{\text{abs}} = \frac{P}{J} = 4\pi \frac{\omega}{c} \operatorname{Im} \alpha(\omega) \tag{6.1.49}$$

Thus, absorption of radiation by a spherical particle is determined by its polarizability. On the other hand, this takes place because the dielectric permittivity ε in the region of particle location differs from that in a surrounding space. Hence, the dielectric permittivity of a particle matter is connected with its polarizability. Let us determine this connection for a spherical particle which radius r_o is large compared to the wavelength. One can use the Poisson's equation for the electric potential φ is $\Delta\varphi = 0$ under these conditions both inside, and outside the particle. The boundary condition for the normal component of the electric displacement near the particle surface has the form

$$\varepsilon \frac{\partial \varphi(R \to r_o - 0)}{\partial R} = \frac{\partial \varphi(R \to r_o + 0)}{\partial R}, \tag{6.1.50}$$

where R is a distance from a particle center, r_o is a particle radius, and ε is its dielectric permittivity. An electric field induces a particle dipole moment $\mathbf{D}$ is connected with the cluster polarizability as $\mathbf{D} = \varepsilon \mathbf{E}$. This leads to the electric field potential φ outside the particle which is induced by the electric field and by the particle dipole moment

$$\varphi = -\mathbf{E}\mathbf{R} + \frac{\mathbf{D}\mathbf{R}}{R^3} \tag{6.1.51}$$

Since the electric potential inside the cluster is restricted, the solution of the Poisson's equation $\Delta\varphi = 0$ may be represented in the form

$$\varphi = C\mathbf{ER}, \tag{6.1.52}$$

where C is a numerical coefficient. This coefficient and the polarizability of the particle can be found from the condition of continuity of the electric potential φ. This gives

$$C = \frac{3\varepsilon}{\varepsilon + 2}; \ \alpha = \frac{\varepsilon - 1}{\varepsilon + 2} a^3 \tag{6.1.53}$$

This relation between the polarizability and its cluster dielectric permittivity holds true also for an alternating electric field $\mathbf{E}_0 \cos \omega t$, where it has the form

$$\alpha(\omega) = \frac{\varepsilon(\omega) - 1}{\varepsilon(\omega) + 2} a^3, \tag{6.1.54}$$

Let us consider the classical limit of scattering of electromagnet wave, where the radiation intensity as a result of scattering is given by formula (1.2.30), i.e.

$$I(t) = \frac{2}{3c^3} \left[\ddot{\mathbf{D}}(t)\right]^2 = \frac{2\omega^4}{3c^3} \alpha^2(\omega) E^2 \tag{6.1.55}$$

The cross section of scattering σ_s is the ratio of this quantity by the energy flux $E^2/4\pi$ of the incident radiation that is given by the Rayleigh formula

$$\sigma = \frac{8\pi\omega^4 \alpha(\omega)^2}{3c^4} \tag{6.1.56}$$

6.2 Absorption of Radiation by Metal Particles

6.2.1 Interaction of Metal Particles with the Electromagnetic Wave

Interaction between an electromagnetic wave and a metal particle is determined, in the first place, by interaction with valence electrons of the metal. We first consider such an interaction with a large particle which may be considered as a metal piece. We give in Table 4.2 electron parameters which influence on the interaction of univalent metals with the electromagnetic wave. In this case valence electrons of atoms become metal valence electrons in the metal formation from atoms. Along with the frequency ω of an electromagnetic wave, one can construct two frequency parameters, namely, the plasma frequency $\omega_p = \sqrt{4\pi N_e e^2/m_e}$ and the metal conductivity Σ.

In order to understand relation between these values, we consider two cases. The first case corresponds to the interaction of visible light with a metal surface. The wavelength of the green color wave is $\lambda = 0.5\,\mu\text{m}$, and its frequency equals $\omega = 3.7 \cdot 10^{16}\,\text{s}^{-1}$. Comparing with data of Table 4.2, we have

$$\omega_p \gg \omega \gg \Sigma \tag{6.2.1}$$

Another example relates to emission from a metal surface at the temperature $T = 1000\,\text{K}$. According to the Wien law, the emission maximum corresponds to the wavelength $\lambda = 0.29\,\mu\text{m}$, and its frequency equals $\omega = 3.7 \cdot 10^{16}\,\text{s}^{-1}$, and we obtain the same relation between the above frequencies. Therefore we ignore below the plasma frequency and consider only parameters ω and Σ which determine the interaction of radiation with a metal particle.

In the case of metal objects the interaction with an electromagnetic wave proceeds through valence electrons; therefore this interaction is stronger than that involving dielectric particles. The skin effect takes place for large particles, so that valence electrons in the metal screen the field of the electromagnetic wave. Hence, the interaction occurs in the metal region near the metal surface; thus, scattering of an electromagnetic wave by a small metal particle is analogous to that in the case of a bulk metal (Table 6.1).

Hence, one can use formulas for scattering of radiation and emission by a small metal particles on the basis of that for bulk metal which are considered in detail in [8]. One can construct these formulas with using a small parameter $\alpha = \omega/2\pi\Sigma$. In this case the penetration depth δ is given by [8]

$$\delta = \frac{\lambda}{(2\pi)^{3/2}}\sqrt{\frac{\omega}{\Sigma}}, \tag{6.2.2}$$

and the particle radius $r_o \gg \delta$. The electric and magnetic fields of the electromagnetic wave decrease inside the metal as $\exp(-z/\delta)$ where z is the distance from the plane boundary inside the metal. Correspondingly, the absorption cross section σ_a of a electromagnetic wave by the metal particle is [8]

Table 6.1 Parameters of univalent metals at room temperature due to valence electrons [7]. Here ρ is the metal mass density, N_e is the number density of valence electrons in the metal, Σ is the metal conductivity, $\omega_p = \sqrt{4\pi N_e e^2/m_e}$ is the plasma frequency for electrons of the metal, so that e, m_e are the electron mass and charge correspondingly

Parameter/metal	Li	Na	K	Cu	Rb	Ag	Cs	Au
ρ, g/cm^3	0.53	0.97	0.89	9.0	1.5	10.5	1.9	19
N_e, $10^{22}\,\text{cm}^{-3}$	4.6	2.5	1.4	8.5	1.1	5.8	0.87	5.9
Σ, $10^{16}\,\text{s}^{-1}$	9.7	19	12	54	7.0	57	4.4	40
ω_p, $10^{16}\,\text{s}^{-1}$	1.2	0.90	0.66	1.6	0.58	1.4	0.53	1.4

$$\sigma_a = \pi r_o^2 \kappa(\alpha),\ \kappa(\alpha) = \sqrt{\frac{\alpha}{2}}\left[\ln\left(\frac{1}{\alpha}\right) - \frac{\pi}{2} + 1\right],\ \alpha = \frac{\omega}{2\pi\Sigma} \ll 1, \qquad (6.2.3)$$

where $\kappa(\alpha)$ is the gray coefficient for the metal surface. Correspondingly, the flux of thermal radiation I_ω from the particle surface is given by

$$I_\omega = I_\omega^{(0)} \kappa(\alpha), \qquad (6.2.4)$$

where $I_\omega^{(0)}$ is the radiative energy flux of the black body (the Planck's radiation).

In particular, the conductivity of silver is $\Sigma = 5.5 \cdot 10^{17}\,\mathrm{s}^{-1}$ at the temperature $T = 300$ K, and $\Sigma = 6.6 \cdot 10^{16}\,\mathrm{s}^{-1}$ at the temperature $T = 2000$ K. According to the Wien's law, the optimal radiation frequency at the temperature $T = 2000$ K is $\omega_{\max} = 1.3 \cdot 10^{15}\,\mathrm{s}^{-1}$. At this temperature a small parameter is $\alpha = 3.1 \cdot 10^{-3}$, that gives for the gray coefficient $\kappa = 0.16$.

6.2.2 *Absorption of Radiation by Metal Nanoparticles*

A size of metal nanoclusters is small compared to the penetration depth for an electromagnet wave, and these particles are uniform in the interaction with radiation. Electrons of metal nanoclusters and microparticles can spread freely over the particle and interact with an electromagnetic wave as free charges. There are two ways of the behavior of the electron subsystem in this interaction. First, the electron subsystem of the particle partakes in interaction as a whole, so that collective properties of the electron subsystem determine absorption of an electromagnetic wave by a metal particle. Second, the spectrum of metal atoms usually includes radiative transitions in a visible spectral range. These spectral lines are broadening in a condensed metal due to the interaction with neighboring atoms which consist partially of ions and electrons. But a general character of radiative transitions in atoms may be conserved in the system of bound atoms. The choose between these two types of interaction involving valence electrons can be done on the basis of experimental data.

A cluster is a system of a finite number of bound atoms. We consider here the metal clusters consisting of large number of bound atoms. This cluster is a uniform particle of a spherical shape where valence electrons can freely propagate inside a cluster volume. However, a cluster size is small compared to a depth of the skin-layer in a bulk metal, and therefore the cross section for interaction of clusters with an electromagnetic wave is proportional to the number of atoms in the cluster, i.e., to the number of valence electrons.

In addition, a cluster radius r_o is small compared to the radiation wavelength λ

$$r_o \ll \lambda \qquad (6.2.5)$$

Considering a metal cluster as a macroscopic system, we take the cluster polarizability to be proportional to the number of its atoms. In addition, for this metal

particle the following criterion holds true

$$\omega \ll \Sigma, \tag{6.2.6}$$

where Σ is the specific conductivity of the cluster matter. This criterion allows one to reduce the problem to the stationary case, where the stationary polarizability of the spherical cluster is $\alpha = r_o^3$. Accordingly, formula (6.1.30) for the absorption cross section may be represented as

$$\sigma_{\text{abs}} = \frac{12\pi\omega}{c} \frac{\varepsilon''}{(\varepsilon' + 2)^2 + \varepsilon''^2} r_o^3 = \frac{\pi\omega}{c} r_o^3 g_{sph}(\omega); \; g_{sph}(\omega) = \frac{12\varepsilon''}{(\varepsilon' + 2)^2 + \varepsilon''^2} \tag{6.2.7}$$

Here the dielectric permittivity of the cluster matter is taken in the form $\varepsilon(\omega) = \varepsilon'(\omega) + i\varepsilon''(\omega)$ It is seen that the absorption cross section by a spherical macroscopic cluster may be estimated as

$$\sigma_{\text{abs}} \sim \frac{r_o}{\lambda} \pi r_o^2,$$

i.e., this cross section is small compared to the geometrical cross section πa^2.

We now apply the above results for metal clusters contained of a finite number of bound atoms. The absorption process is determined by valence cluster electrons. Assuming that these electrons are free, under criterion (6.2.5), the dielectric permittivity of an electron plasma is given by

$$\varepsilon(\omega) = 1 - \frac{\omega^2}{\omega_p^2} \tag{6.2.8}$$

Here ω_p is the plasma frequency or Langmuir frequency, that is given by the expression

$$\omega_p = \sqrt{\frac{4\pi N_e e^2}{m_e}},$$

where N_e is the electron number density, e and m_e are the electron charge and mass, respectively. Assuming that $\varepsilon'' \ll 1$, we transform formula (6.2.7) taking into account the expression (6.2.8) near the resonance frequency

$$\sigma_{\text{abs}}(\omega) = 2\pi \frac{\hbar\omega^2}{c} a^3 \frac{\Gamma}{\hbar^2(\omega - \omega_0)^2 + \Gamma^2} = \sigma_{\max} \frac{\Gamma^2}{\hbar^2(\omega - \omega_0)^2 + \Gamma^2}, \tag{6.2.9}$$

where ω_0 is the resonance Mie frequency,

$$\omega_0 = \frac{\omega_p}{\sqrt{3}},$$

Γ is the resonance width according to

$$\Gamma = \frac{\hbar\omega_0\varepsilon''}{6},$$

and $\sigma_{\max}$ is the maximum absorption cross section,

$$\sigma_{\max} = 2\pi\frac{\hbar\omega^2}{\Gamma c}a^3. \tag{6.2.10}$$

From formulas (6.2.9) and (6.2.10) it follows the integral relation

$$\int \sigma_{\text{abs}}(\omega)\mathrm{d}\omega = \pi\sigma_{\max}\frac{\Gamma}{2\hbar} \tag{6.2.11}$$

where the resonance width is assumed to be relatively small. Within the frame of liquid drop model, the cluster radius is given by [9, 10]

$$r_o^3 = r_w^3 n,$$

where r_w is the Wigner-Seitz radius, and n is the number of cluster atoms. Under used conditions, the cluster is assumed to be a uniform particle, and the absorption cross section is proportional to the number of cluster atoms.

Though the above cluster model of a uniform spherical particle is rough, it is convenient to demonstrate the mechanisms of cluster absorption through the interaction between an electromagnetic field and valence electrons which leads to the resonance character of the absorption cross section as a function of a photon frequency. In practice, the absorption spectrum has more complex structure, and it can include several peaks. Table 4.3 contains parameters of the absorption cross sections for some metal clusters for which these cross sections can be approximated by a simple resonance dependence. Basing on the experimental data [11–14] for the cross sections of absorption by clusters consisting of Li, K and Ag atoms, one can check the validity of the plasma model for the absorption cross section of clusters. It is convenient to introduce the parameter

$$\xi = \sigma_{\max}\frac{\Gamma c}{2\pi\hbar\omega_0^2 a^2}, \tag{6.2.12}$$

that is equal to one, if formula (6.2.9) is correct.

As it follows from Table 6.2, the parameter ξ differs from one stronger than the limits of its accuracy. This means violation of the macroscopic character of absorption in accordance with formula (6.2.7) and prohibits to describe valence electrons as free ones that leads to formula (6.2.9) for the absorption cross section. Thus, the concept of the interaction of the electromagnetic wave with cluster electrons as plasma ones is violated.

One more comparison confirms this conclusion. The resonance frequency for metal clusters with one valence electron per atom which are given in Table 6.2 is equal to

Table 6.2 Parameters of the absorption cross sections for metal clusters

Cluster	$\hbar\omega_0$, eV	Γ, eV	$\sigma_{\max}/n$,Å^2	ξ	β	f
Li^+_{139}	2.92	0.90	62	2.8	0.24	0.58
Li^+_{270}	3.06	1.15	120	3.2	0.30	0.73
Li^+_{440}	3.17	1.32	280	4.9	0.50	1.20
Li^+_{820}	3.21	1.10	440	3.3	0.52	0.85
Li^+_{1500}	3.25	1.15	830	3.5	0.66	0.91
K^+_9	1.93	0.22	26	2.9	0.27	0.91
K^+_{21}	1.98	0.16	88	2.9	0.52	0.96
K^+_{500}	2.03	0.28	1750	4.0	1.3	1.40
K^+_{900}	2.05	0.40	2500	4.5	1.2	1.59
Ag^+_9	4.02	0.62	8.84	2.6	0.24	0.87
Ag^+_{21}	3.82	0.56	16.8	2.1	0.26	0.64

$$\omega_0 = \omega_p/\sqrt{3} = \frac{e}{\sqrt{m_e r_W^3}}$$

The number density of valence electrons is equal to

$$N_e = \frac{3}{4\pi r_W^3},$$

where r_W is the Wigner-Seitz radius. The value of $\hbar\omega_0$ is equal to 13.5 eV for large Li clusters, to 7.1 eV for large K clusters, and to 14.7 eV for for large Ag clusters. A large difference of these data from measured values of Table 6.2 allows us to conclude that the plasma model for valence electrons in the analysis of absorption of an electromagnetic wave by metal clusters is incorrect. In addition, we show in Fig. 6.4 experimental dependencies for the absorption cross sections of some Ag clusters on the photon frequency. As it is seen, the absorption cross sections can contain both one and two resonance maxima. This is also rejects the plasma model for valence electrons.

We now consider the sum rule for a metal cluster. At fixed nuclei the absorption spectrum of the cluster consists of a finite number of spectral lines; the number of these lines is comparable with the number of cluster valence electrons. In the limit of one atom this spectrum is transformed into one or several resonance spectral lines. Let us introduce the effective oscillator strength f per one valence electron. Then the total oscillator strength is equal to nf, where n is the number of valence electrons in the cluster. Due to nuclear motion, the absorption spectrum of clusters is transformed from set of separate spectral lines into the continuous curve. However, the sum of the oscillator strengths does not change. One can expect that the effective oscillator strength f per one atom depends weakly on the cluster size, and it corresponds to

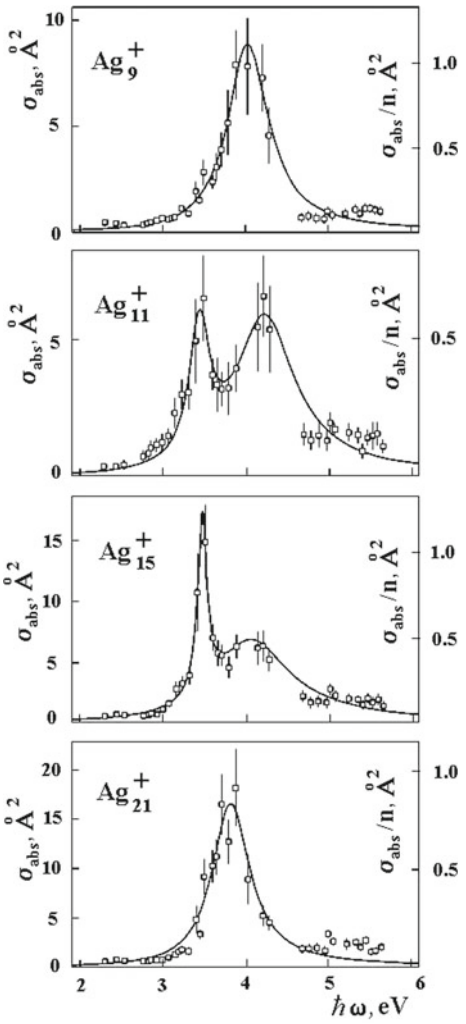

Fig. 6.4 Absorption cross sections for silver clusters [14]

the atomic value. Below we check this concept using the analysis of clusters with a plasma form of the absorption cross section which are contained in the Table 6.2.

Let us use the general expression for the cross section of photon absorption by an atomic system in the form

$$\sigma_{\text{abs}}\,(i \to j) = \frac{\pi^2 c^2}{\omega^2}\frac{a_\omega}{\tau_{\text{ij}}}\frac{g_j}{g_i} = \frac{2\pi^2 c^2}{m_e c} f_{\text{ij}} g_k a_\omega \tag{6.2.13}$$

Here ω is the frequency of a given electron transition between states i (the lower state) and j (the upper state); g_i, g_j are statistical weights of these transition states, τ_{ij}

is the radiative lifetime with respect to this transition, a_ω is the frequency distribution function for the radiated photons which is normalized as (2.1.1)

$$\int a_\omega \mathrm{d}\omega = 1;$$

finally, f_{ij} is the oscillator strength for this transition. The sum rule for dipole radiation transitions of valence electrons in the spectral range including resonance transitions, is of the form

$$\int \sigma_{\mathrm{abs}}(\omega)\mathrm{d}\omega = \frac{2\pi^2 e^2}{m_e c} nf \tag{6.2.14}$$

This sum rule is analogous to those for atoms (1.3.11).

If the absorption cross section has a resonance structure, analogously to that for clusters in Table 6.2, the integral relation (6.2.11) is also applicable. Then it follows from relations (6.2.11) and (6.2.14) that

$$f = \frac{\sigma_{\max}\Gamma m_e c}{2\pi^2 e^2 n\hbar} \tag{6.2.15}$$

The values of the effective oscillator strength for metal clusters with resonance structure of absorption are given in Table 6.2. Different values for each element are explained, in our opinion, by a restricted accuracy of used data. Average values of the oscillator strength for each cluster correspond to oscillator strengths of low-lying transitions ${}^2S_{1/2} \rightarrow {}^2P_{1/2} \rightarrow {}^2P_{3/2}$ of their atoms. The total oscillator strengths are equal to 0.74 for the lithium atom, 1.5 for the potassium atom, and 0.77 for the silver atom. Coincidence of the oscillator strengths for clusters with corresponding values for atoms confirms the fact that the absorption spectra of clusters can be obtained by transformations of atomic resonance lines due to the interaction between atoms and due to the nuclear motion.

In considering of the interaction of metal clusters with the radiation field, on the one hand, these clusters are uniform with respect to radiation, and on the other hand, they may be considered as macroscopic ones, where the interaction with an electromagnetic field is determined by the electron subsystem. Let us construct this cluster from n bound metal atoms and transfer an electron of one of these atoms into the resonance excited state by means of the dipole radiative transition, so that the oscillator strength of this transition is of the order of one. This excitation is spread over the cluster, and the spectrum of cluster excitation consists of n discrete spectral lines. The total spectrum of cluster excitation with accounting for atom motion has a continuous structure with one or several maxima. This form of the cluster spectrum follows also from computer simulations, and the integral absorption cross section is proportional to the number of valence electrons.

6.2.3 Emission of Metal Clusters in Hot Gases

A strong interaction between metal clusters and resonance radiation may be of importance both for radiative properties of metal clusters located in a buffer gas and for the heat balance of this system. We below determine the spectral radiation power $p(\omega)$ of a cluster at a certain temperature T. This spectral power is expressed through the absorption cross section σ_{abs} according to the Kirchhoff law as

$$p(\omega) = \hbar\omega \cdot I(\omega) \cdot \sigma_{\text{abs}}(\omega) \ , \tag{6.2.16}$$

where in accordance with formula (2.2.7) $I(\omega)$ is the isotropic flux of the black body radiation at a given frequency and temperature

$$I(\omega) = \left(\frac{\omega}{\pi c}\right)^2 \frac{1}{\exp\left(\hbar\omega/T\right) - 1} \tag{6.2.17}$$

Here $\sigma_{\text{abs}}(\omega)$ is the absorption cross section for a given cluster as a small particle. From this it follows that the spectral radiative power by a small cluster has the form

$$p(\omega) = \frac{\hbar\omega^3}{\pi^2 c^2} \frac{\sigma_{\text{abs}}(\omega)}{\exp\left(\hbar\omega/T\right) - 1} \tag{6.2.18}$$

In particular, the total radiation power of a small macroscopic particle with a radius a is [15, 16]

$$P = \int_0^\infty p(\omega)\mathrm{d}\omega = \frac{12\pi}{\hbar c} a^3 g\sigma T^5 \kappa = \frac{46\pi a^3 g\sigma T^5}{\hbar c}; \ \frac{Ta}{\hbar c} \ll 1 \tag{6.2.19}$$

Here the quantity

$$g = \frac{\varepsilon''}{(\varepsilon' + 2)^2 + (\varepsilon'')^2}$$

is given by formula (6.2.7) and is assumed to be independent on the frequency; σ is the Stephan-Boltzmann constant, and the numerical coefficient is $\kappa = 3.83$. It is seen that the radiation power by a small macroscopic particle under equilibrium conditions is proportional to T^5, in contrast to the classical dependence $\sim T^4$ for the radiative power of a macroscopic black body surface.

According to formula (6.2.7) and (6.2.14), the absorption cross section for a small cluster is proportional to the number of cluster atoms. Hence, the specific absorption cross section, i.e., the absorption cross section by one atom, does not depend on the cluster size. Therefore, the cluster radiative power per unit volume is proportional to the number density of bound atoms. This statement does not depend on the distribution function of clusters, or of small particles over their sizes. Thus, the total radiation power for a given volume of a gas, or of a plasma, is determined

Table 6.3 The specific radiation power P_{rad}, 10^7 W/g, and the light yield for large clusters at various temperatures, expressed in lm/W and given in parentheses

Cluster	3000 K	3500 K	4000 K
Ag	0.71 (51)	1.6 (25)	3.5 (88)
K	4.0 (106)	8.6 (111)	17 (165)
Li	2.0 (51)	4.9 (80)	10 (102)
Black body	(22)	(39)	(57)

by the total number of bound atoms, and it does not depend on the size of the cluster. This general conclusion is based on the statement that absorption cross section is proportional to the number of bound atoms and it is valid both for clusters and small macroscopic particles.

We now use parameters of the absorption cross sections for lithium, potassium and silver clusters given in Table 6.2 in order to analyze numerically the radiative parameters of the plasma which contains clusters. Table 6.3 presents the specific radiation powers for clusters; they are determined by the expression

$$P_{\text{rad}} = \int \frac{p\,(\omega)\,\mathrm{d}\omega}{M}, \tag{6.2.20}$$

where M is the cluster mass. Here we take into account that the radiation power is proportional to the total mass of bound radiating atoms in clusters. Table 6.3 contains also (in brackets) the light yield of cluster radiation where the absorption cross sections for these clusters are used as model ones. The light radiation yield characterizes the efficiency of the eye perception that is given by the expression

$$\eta = \frac{\int p(\omega) V\,(\omega)\mathrm{d}\omega}{\int p(\omega)\mathrm{d}\omega}, \tag{6.2.21}$$

where the spectral radiation power $p(\omega)$ is calculated on the basis of formula (6.2.18), and the visibility function $V\,(\omega)$ determines the perception of radiation by eye; this function has maximum about of 683 lm/W for the wavelength of radiation of $\lambda = 555\,\text{nm}$. For comparison, Table 6.3 contains also the light yield of the black body. It is seen that clusters as light sources are better than a black body because of a more favorable radiation spectrum (a thermal infrared radiation is excluded from the radiation spectrum of the clusters). It follows from data of the Table 6.3 that at the temperature of $T = 3600$ K the averaged radiation power of the clusters is $1 \cdot 10^8$ W/g. This value is convenient for estimates.

Thus, metal clusters or small macroscopic particles which are located in a hot, or ionized gas, can be responsible for radiation of these systems. For example, this occurs in the flame where radiation is produced by small soot particles.

6.3 Absorption by Atmospheric Particles

6.3.1 Aerosols and Water Microdrops in Atmosphere

Aerosols are particles of nano-sized and micro-sized particles located in the atmosphere [17–22]. Sometimes water microdrops which form clouds and are of importance in electric and radiative properties of the Earth's atmosphere, are included in the list of aerosols [23, 24]. Below the object of our consideration will be just water drops as an important atmospheric radiator in the infrared spectrum range [25–28]. But first we glance at aerosols as small particles which are influenced by atmospheric properties.

Figure 6.5 contains various types of nanoparticles and microparticles which can be presented in atmospheric air. For comparison, nanoclusters and electric probes are added to this list, though these objects exist irrespectively the atmosphere. Aitken particles were investigated from 19th century [30–33], earlier than other atmospheric particles. They are located at high altitudes, above clouds, and their basis are radicals of sulfur compounds which result from vaporization of meteorites at high altitudes and from processes which proceed at the Earth surface or in the atmosphere at low altitudes. Since their size is below 0.1 μm, Aitken particles are also responsible for a blue sky color because shortwave photons scatter on these particles effectively. The number density of Aitken particles at altitudes 10–20 km is $10^2 - 10^4\,\mathrm{cm}^{-3}$ [34].

Aerosols at low altitudes results from processes which proceed at the Earth's surface. Sulfur SO_x and nitrogen NO_x oxides, as well as atmospheric ions, are nuclei of condensation in formation of water microdrops. In addition, sulfur and nitrogen

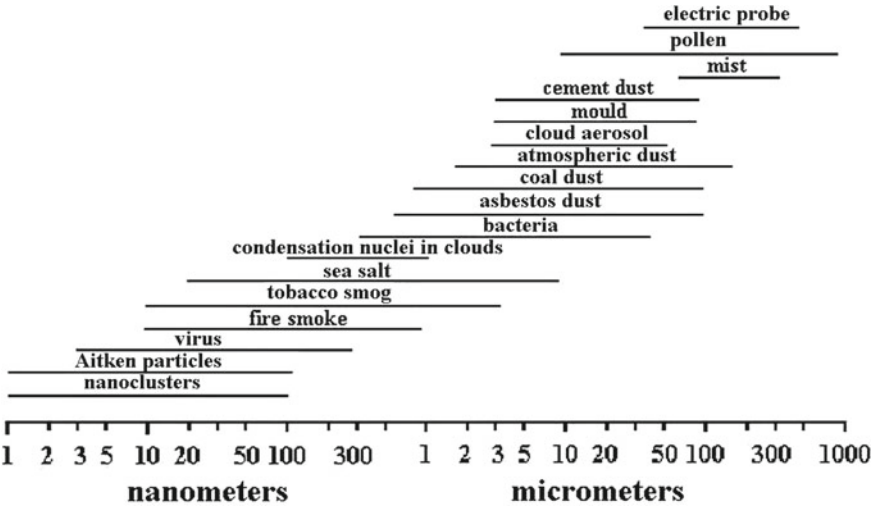

Fig. 6.5 Typical size of aerosols and microparticles located in the Earth atmosphere [29]

oxides, as well as soot particles, are formed in processes of combustion of solid and liquid organic compounds in air. A large amount of aerosols is formed as a result of volcano eruption. Some part of particles in atmospheric air goes up from the Earth's surface under the wind action. The putrefaction processes at the Earth's surface cause extraction of some aerosols and their transport to the atmosphere. In spite of the variety of aerosols located in atmospheric air in accordance with Fig. 6.5, they do not influence radiative properties of the atmosphere because of a small amount.

The Earth's atmosphere contains a large amount of atmospheric water which results from circulation of water in the nature. Water circulation consists of water evaporation from open water reservoirs at the Earth's surface and rain or snow return water back to the Earth's surface. This process establishes the amount of atmospheric water $1.3 \cdot 10^{19}$ g [35–38], and the total rate of water evaporation from the Earth's surface is $3.9 \cdot 10^{20}$ g/yr [39–42]. Precipitation of atmospheric water on the Earth's surface with uniform distribution over it gives a layer of liquid water of a thickness 2.5 cm [43]. The average concentration of water molecules in atmospheric air as approximately 0.4%, whereas near the Earth's surface the average concentration of water molecules in air is equal 1.7%, i.e. the number density of atmospheric water molecules decreases sharper with an altitude increase than that for air molecules. An average time of residence of water molecules in the atmosphere is approximately 9 days [42]. These data are the basis to analyze the atmospheric greenhouse phenomenon.

A small part of atmospheric water is found in the atmosphere in the form of water microdrops which interact effectively with infrared radiation. Near the Earth's surface, the average partial pressure of water is about 2 *Torr*, whereas the saturated water pressure is 4.7 *Torr* at the surface temperature [44, 45]. Therefore atmospheric water is in the form of a vapor consisting of free molecules mostly, and a small part of water exist in the form of aerosols, at least, at altitudes below 3 km. Aerosols are formed and exist at larger altitudes; processes with their participation [21, 26–28, 46, 47] are important for optic and electric atmospheric properties. Formation of aerosols may proceed if the partial pressure of water exceeds the saturated vapor pressure at a current atmosphere temperature which is taken from [45]. The ratio of these pressures is the air moisture. There are reliable methods of measurements of the global moisture (for example, [48, 49]) which allows one to analyze the evolution of the moisture of atmospheric air at some altitudes in time.

Atmospheric water is the main greenhouse component and includes a water vapor consisting of free water molecules and water aerosols which compose clouds. Figure 6.6 gives the absorption spectrum of liquid water. As is seen, the absorption coefficient in the visible spectral range is lower by seven orders of magnitude compared with that in the infrared spectral range. This means that water aerosols are transparent for solar radiation, and clouds are seen due to absorbed admixtures, whereas these microdrops are sources of IR radiation. Let us estimate the role of water aerosols in IR emission of the atmosphere taking the cross section of absorption of an infrared photon $\sigma = \pi r^2$ under the criterion $\lambda \leq r$, where r is a drop radius, and λ is the wave length. Correspondingly, the optical thickness u of the layer with the depth l and number density N of water microdrops is equal

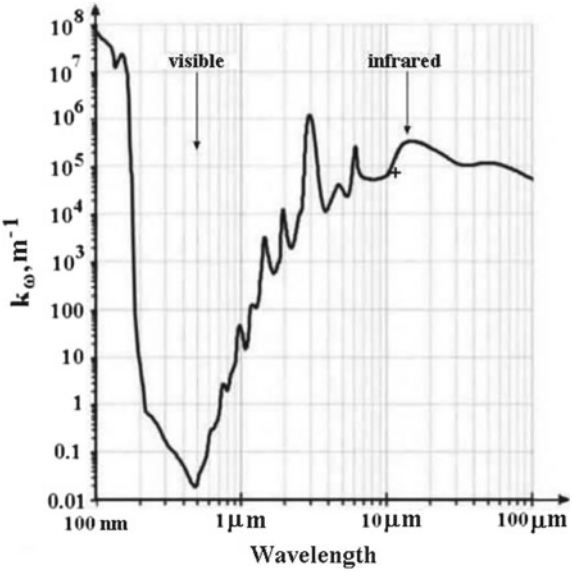

Fig. 6.6 Absorption coefficient for a bulk liquid water layer under normal conditions [50]. A cross indicates the absorption coefficient for aerosols [51]

$$u = \pi r^2 N l, \tag{6.3.1}$$

and the water mass in aerosols per unit square of the Earth's surface m is

$$m = \frac{4}{3}\pi r^3 N l = \frac{4ru\rho}{3}, \tag{6.3.2}$$

where ρ is the water density. One can see that the observed optical thickness of the atmosphere ($u \approx 3$) may be provided by approximately 0.2% of atmospheric water if it is located in the form of liquid microdrops-aerosols.

Let us note two types of interaction of an electromagnetic wave with a dielectric particle. Above we considered the case when this interaction results from electric properties of a particle material which is described by its dielectric constant. Another character of this interaction consists in absorption of radiation by this particle due to transitions between molecular states of this particle and also due to transitions between states owing to interaction between molecules of this condensed matter. Evidently, the absorption coefficient of Fig. 6.6 for liquid water in the infrared spectrum range is determined by such transitions.

Let us analyze also the result of experiment [51] which is given in Fig. 6.6 according to which water microdrops of an average radius $r = 10\,\mu\text{m}$ are characterized by the absorption cross section $\sigma_{\text{abs}} = \pi r^2$ for thermal atmospheric radiation. Then the optical thickness u of a layer of a thickness l is equal at the number density N of microdrops

$$u = Nl\sigma_{\text{abs}} = Nl\pi r^2$$

From the another standpoint, the mass per unit area $M = \rho l$ is

$$M = Nl \cdot \frac{4}{3}\pi r^3 \rho,$$

where ρ is the mass density of water. On the basis of these formulas, the absorption coefficient is equal to

$$k_\omega = \frac{u}{l} = \frac{3\sigma_{\text{abs}}}{4r^3}$$

Under the above considered conditions ($\sigma_{\text{abs}} = \pi r^2$) the absorption coefficient $k_\omega \sim 10^5\ \text{m}^{-1}$ (it is included in Fig. 6.6 shows the identity of the absorption coefficient for liquid water and a gas of water microdrops).

6.3.2 *Water Microdrops in Clouds*

Considering an interaction of an individual atmospheric water microdrop with atmospheric radiation and being guided by experiment [51], we take a drop radius to be $r = 10\,\mu\text{m}$. In this case the absorption cross section of thermal atmospheric radiation $\lambda \sim r \approx 10\,\mu\text{m}$ by a given microdrop is close to its geometric cross section; it is equal to $\sigma_{\text{abs}} \sim 3 \cdot 10^{-6}\,\text{cm}^2$, whereas for solar radiation the absorption cross section is equal $\sigma_{\text{abs}} \sim 10^{-11}\,\text{cm}^2$. In order to analyze radiative parameters of a microdrops in a cumulus, we take typical parameters of water microdrops in cumulus as [52–55])

$$r_o = 8\,\mu\text{m},\ N_d = 10^3\text{cm}^{-3}, \tag{6.3.3}$$

where r_o is the average drop radius, and N_d is an average density of water microdrops in cumulus in a thunderstorm weather. This gives for the absorption coefficient $k_\omega = \sigma_{\text{abs}} N_d \sim 10^{-3}\,\text{cm}^{-1}$, and a typical observed optical thickness $u = k_\omega L$ of cumulus corresponds to its thickness $L \sim 30\text{m}$.

One can see according to Fig. 6.6 data, that the cloud optical thickness in the visible spectrum range is equal $u \sim (10^{-4} - 10^{-3})$, i.e. a cloud is transparent for visible radiation. Hence, clouds in the course of their formation are invisible. Through a time they become visible as a result of attachment of absorbed components, in particular, a dust or optically active atoms in the visible spectrum range. Below we estimate an amount of sodium atoms in a drop which provide absorption of visible radiation. Sodium atoms are formed in a drop as a result of attachment of molecules NaCl to this drop or joining of this drop with a small particle of this salt.

We assume that injection of sodium atoms into a water microdrop leads to broadening of an absorption line, so that it is transformed in an absorption band of a width $\hbar\Delta\omega \sim 1\text{eV}$. According to formula (2.2.24) the absorption cross section may be estimated as

$$\sigma_{\text{abs}} = \frac{\lambda^2}{4\Delta\omega\tau}, \tag{6.3.4}$$

where a typical wavelength in the visible spectrum range is $\lambda \sim 0.5\,\mu\text{m}$. Taking a typical lifetime for an upper state of transition is $\tau \sim 10^{-8}\,\text{s}$. This gives a typical absorption cross section $\sigma_{\text{Na}} \sim 5 \cdot 10^{-17}\text{cm}^2$. Let a drop contains n sodium atoms, and then a cloud becomes nontransparent in a visible spectrum range, if its optical thickness is

$$u = NLn\sigma_{\text{Na}} \sim 1$$

From this consideration we have $n \sim 6 \cdot 10^9$. Because an individual microdrop contains $n = 7 \cdot 10^{13}$ water molecules, one can find a typical concentration of sodium atoms in water, that is, ~0.01%. This amount of sodium solved in water provides the visibility of clouds in a sky.

Though it is known that the covering of a sky by clouds is approximately 70%. But this does not mean that the other part of sky is not occupied with water microdrops. Indeed, at the first stage of the nucleation process that leads to conversion of water molecules in water microdrops transparent drops are formed, and only through a time they become visible after attachment of absorbed atoms or dust particles to microdrops.

Let us take the cross section of absorption σ_{abs} by an aerosol particle of a radius r to be [16]

$$\sigma_{\text{abs}} = \pi r^2, \tag{6.3.5}$$

if an aerosol radius is large compared to the wavelength of radiation λ. In other limiting case we have [8]

$$\sigma_{\text{abs}} \sim \frac{r^3}{\lambda}, \; r \ll \lambda \tag{6.3.6}$$

From this one can construct the absorption cross section by an aerosol particle as a function of an aerosol size in the form

$$\sigma_{\text{abs}} = \frac{\pi r^2}{1 + C\frac{\lambda}{r}} \tag{6.3.7}$$

From the above experimental data it follows that in this frequency range formula (6.3.5) holds true with an accuracy of 20%, and the cross section of absorption of thermal radiation by aerosols of a radius (8–10) μm is $(2.5 \pm 0.5) \cdot 10^{-6}\text{cm}^2$.

This leads to the depth of a formed water layer (30–40) μm that corresponds to the concentration of atmospheric water in aerosols roughly $(1 - 2)\%$. It is seen that water aerosols may give a remarkable contribution to atmospheric emission. This result causes alarm with respect to the climate change because transition of a small part of an atmospheric water vapor in aerosols may lead to a significant change of the atmospheric optical thickness. In particular, according to studies [56–59] cosmic rays influence on formation of aerosols and clouds in the Earth's atmosphere.

Thus, we have that the spectral radiative flux of the Earth's atmosphere may include some frequency bands which are created by vibration-rotation or rotation radiative transitions of certain components. One can introduce the effective temper-

ature for a certain frequency band in accordance with formula (7.1.17). The optical thickness of the atmosphere starting from this layer in the direction perpendicular to the Earth surface equals to 2/3 at a given frequency, and the temperature of this atmospheric layer is the radiative temperature for emission at a given frequency. We below use this concept in the analysis of emission of atmospheric CO_2 molecules.

Note that clouds consisting of water aerosols water aerosols influence on the Earth's energetics. In accordance with Fig. 6.6, the absorption of radiation by water aerosols is strong for the infrared spectrum range, whereas water aerosols are transparent for visible radiation. But this fact corresponds to pure liquid water, and if some chemical components are dissolved in water, the situation may be changed. Hence, on the first stage of formation of water aerosols they are transparent microdrops, and subsequently after attachment of some impurities water aerosols become visible. One can demonstrate the influence of admixtures on optical properties of aerosols in the case when the sodium salt NaCl is dissolved in water of an aerosol; then the solute sodium atoms determine the absorption of visible radiation by aerosols.

Let us assume that yellow spectral line of absorption of a free sodium atom is converted in an absorbed band as a result of interaction with surrounding water molecules, if a sodium atom is located in water. Taking a width of the absorption band $\Delta\omega$ to be $\hbar\Delta\omega \sim 1\text{eV}$, one can obtain for the absorption cross section σ as a result of interaction of an electromagnetic wave with a dissolved sodium atom

$$\sigma_{\text{vis}} = \frac{\lambda^2}{4} \cdot \frac{1}{\Delta\omega\tau}, \tag{6.3.8}$$

where λ is a wavelength, τ is the radiative lifetime of an excited atom which is estimated as

$$\frac{1}{\tau} = \frac{2e^2\omega^2}{m_e c^3} f g_o \tag{6.3.9}$$

Here m_e is the electron mass, f is the oscillator strength for transition between atomic states, g_o is the statistical weight of the lower transition state which is the ground electron state. Because $f \sim 1$ and $g_o \sim 1$, it follows from formula (6.3.8) an estimate for the absorption cross section

$$\sigma_{\text{vis}} \sim \frac{e^2}{\Delta\omega m_e c} \tag{6.3.10}$$

This formula gives $\sigma_{\text{vis}} \sim 5 \cdot 10^{-18}\,\text{cm}^2$. Let us take for definiteness aerosols of a cumulus clouds with an average radius $r = 8\,\mu\text{m}$ and the absorption cross section $\sigma \approx 2.5 \cdot 10^{-6}\,\text{cm}^2$ for infrared radiation. This cross section may be reached as a result of absorption of dilute sodium atoms if the concentration $c(\text{Na})$ of these atoms in aerosols is $c(\text{Na}) \sim 0.5\%$. These conditions may be attained in reality.

6.3.3 Atmospheric Water Microdrops as Atmospheric Radiators and Absorbers

Water drops are effective radiators and absorbers of infrared radiation. Being located in the Earth's atmosphere, they interact effectively with infrared radiation that passes through the atmosphere. We now consider the energetic balance of an individual water microdrop which interacts with this infrared radiation through processes of emission and absorption; it interacts also with surrounding air through the thermal conductivity process. This microdrop exchange through the thermal conductivity of air; the power P_κ which the drop takes from air or transfers to it in the case of a higher drop temperature compared to the air temperature far from the drop, is equal [15, 16]

$$P_\kappa = 4\pi r_o \kappa \Delta T, \tag{6.3.11}$$

where r_o is a drop radius, κ is the air thermal conductivity, and ΔT is the temperature difference for the drop under consideration and surrounding air far from it. Here we assume that the drop radius r_o is large compared to the mean free path of molecules in air.

Considering a microdrop as a black body, we have the following energetic balance equation

$$4\pi r_o \kappa \Delta T = 4\pi r_o^2 \sigma T^4 - P_{\text{abs}}, \;\; \Delta T = T - T_a, \tag{6.3.12}$$

where σ is the Stephan-Boltzmann constant, T is the drop temperature, P_{abs} is the power absorbed by drop in the form of infrared radiation, T_a is the air temperature. In accordance with Fig. 6.6, we assume that absorbed radiation is emitted at a distance λ from the drop, that is, the mean free path of an infrared photon in atmospheric air; then we obtain for the absorbed power

$$P_{\text{abs}} = 4\pi r_o^2 \int_{-1}^{1} \sigma T (\cos\theta)^4 = 4\pi r_o^2 \int_{-1}^{1} \sigma \left[T + \lambda \frac{\mathrm{d}T}{\mathrm{d}h} \cos\theta \right]^4 = 4\pi r_o^2 \sigma \left[T^4 + 4 \left(\lambda \frac{\mathrm{d}T}{\mathrm{d}h} \right)^2 T^2 \right] \tag{6.3.13}$$

Here $\mathrm{d}T/\mathrm{d}h = 6.5\,\text{K/km}$ is the temperature gradient in the atmosphere, and we take roughly $\lambda \approx 2\,\text{km}$ for infrared radiation. From this we find the difference between temperatures of the drop and surrounding air

$$\Delta T = \frac{4 r_o \sigma T^2}{\kappa} \left(\lambda \frac{\mathrm{d}T}{\mathrm{d}h} \right)^2 \tag{6.3.14}$$

It is seen that the drop temperature is higher than the temperature of surrounding air in the case $h > \lambda$ which is represented in Fig. 6.7. For a drop radius $r_o = 10\,\mu\text{m}$ we take $h = \lambda = 2\,\text{km}$, where the temperature is $T = 270\,\text{K}$ with $\kappa = 2.4\text{W/m}^2$ [45]; then we obtain $\Delta T = 1 \cdot 10^{-5}\,\text{K}$. This value increases if the altitude decreases. In particular, when the microdrop reaches the Earth's surface ($h = 0$), we have instead of (6.3.14)

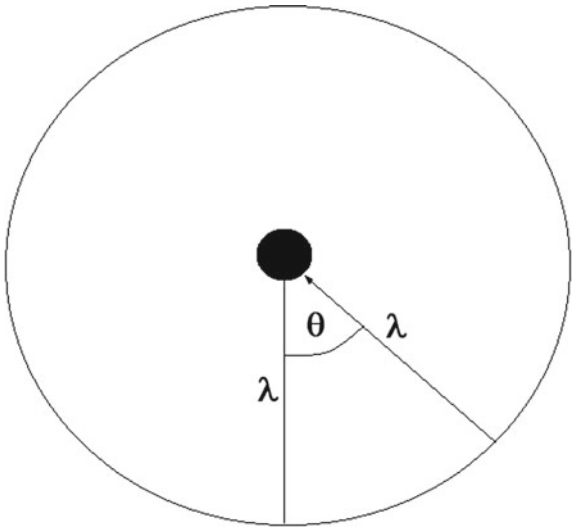

Fig. 6.7 Geometry of a microdrop located in atmospheric air and interacted with passed radiation

$$\Delta T = -\frac{2r_o}{\kappa}\sigma T^3 \lambda \frac{\mathrm{d}T}{\mathrm{d}h} \tag{6.3.15}$$

In this case the drop temperature is lower than that for surrounding air, and $\Delta T = -6 \cdot 10^{-3}$ K. Thus from this analysis one can conclude that if a microdrop is located in atmospheric air, its temperature coincides practically with the temperature of surrounding air.

References

1. L. Long, *The Raman Effect: The Unified Theory of Raman Scattering by Molecules* (Wiley, New York, 1977)
2. N.B. Colthrup, L.H. Daly, S.E. Wiberley, *Introduction to Infrared and Raman Spectroscopy* (San Diego, Academic Press, 1990)
3. P. Hendra, C. Jones, G. Warnes, *FT Raman Spectroscopy* (Ellis Horwood Ltd, Chichester, 1991)
4. J.R. Ferraro, K. Nakamoto, *Introductory Raman Spectroscopy* (Academic Press, San Diego, 1994)
5. R.L. McCreery, *Raman Spectroscopy of Chemical Analysis* (Wiley, New York, 2000)
6. E. Smith, G. Dent, *Modern Raman Spectroscopy. A Practical Approach* (Chichester, Wiley, 2005)
7. B.M. Smirnov, *Reference Data on Atomic Physics and Atomic Processes* (Springer, Heidelberg, 2008)
8. L.D. Landau, E.M. Lifshitz, *Electrodynamics of Continuous Media* (Pergamon Press, Oxford, 1984)
9. E.P. Wigner, F. Seitz, Phys. Rev. **46**, 509 (1934)
10. E.P. Wigner, F. Seitz, Phys. Rev. **46**, 1002 (1934)
11. C. Bréchignac, P. Cahuzac, F. Carlier, J. Leygnier. Chem. Phys. Lett. **164**, 433 (1989)
12. C. Bréchignac, P. Cahuzac, N. Kebaili, J. Leygnier, A. Sarfati, Phys. Rev. Lett. **68**, 3916 (1992)

13. C. Bréchignac, P. Cahuzac, J. Leygnier, A. Sarfati, Phys. Rev. Lett. **70**, 2036 (1993)
14. J. Tiggesburker, L. Köller, H.O. Lutz, K.-H. Meiwes-Broer, Chem. Phys. Lett. **190**, 42 (1992)
15. B.M. Smirnov, *Clusters and Small Particles Processes in Gases and Plasmas* (Springer, New York, 1999)
16. B.M. Smirnov, *Cluster Processes in Gases and Plasmas* (Wiley, New York, 2010)
17. H.R. Byers, *Elements of Cloud Physics* (University of Chicago Press, Chicago, 1965)
18. N.H. Fletcher, *The Physics of Rainclouds* (Cambridge University Press, London, 1969)
19. S. Twomey, *Atmospheric Aerosols* (Elsevier, Amsterdam, 1977)
20. H. Proppacher, J. Klett, *Microphysics of Clouds and Precipitation* (Reidel, London, 1978)
21. M.L. Salby, *Fundamentals of Atmospheric Physics* (Academic Press, San Diego, 1996)
22. B.J. Mason, *The Physics of Clouds* (Oxford Univesity Press, Oxford, 2010)
23. L.S. Ivlev, *Chemical Composition and Structure of Atmosphere Aerosols* (Izd. Leningrad State University, Leningrad, 1982). (in Russian)
24. I.V. Petryanov-Sokolov, A.G. Sutugin, *Aerosols* (Moscow, Nauka, 1989). (in Russian)
25. O. Boucher, *Atmospheric Aerosols. Properties and Climate Impacts* (Springer, Dordrecht, 2015)
26. H.R. Grim, *Plasma Spectroscopy* (Cambridge University Press, New York, 1964)
27. R.G. Flleagle, J.A. Businger, *An Introduction to Atmospheric Physics* (Academic Press, San Diego, 1980)
28. K. Friedlander, *Smoke, Dust, and Haze. Fundamentals of Aerosol Dynamics.* (Oxford University Press, Oxford, 2000)
29. B.M. Smirnov, *Fundamental of Ionized Gases. Basic Topics of Ionized Gases* (Wiley, Weinheim, 2012)
30. J. Aitken, Nature **23**(583), 195–197 (1880)
31. J. Aitken, Nature **23**(588), 311–312 (1881)
32. J. Aitken, Nature **23**(591), 384–385 (1881)
33. J. Aitken, Trans. Roy. Soc. Edinburgh **35**(1), 1–19 (1888)
34. S.H. Harris, in *Encyclopedia of Physics*, ed. by R.G. Lerner, G.L. Trigg (VCH Publisher, New York, 1990, p. 30; Weinheim, Wiley, 2005, p. 61)
35. I.A. Shiklomanov, in *Water in Crisis: A Guide to the World's Fresh Water Resources*, ed. by P.H. Gleick (Oxford University Press, Oxford, 1993), pp. 13–24
36. I.A. Shiklomanov, J.C. Rodda (eds.), *World Water Resources at the Beginning of the Twenty-First Century* (Cambridge University Press, Cambridge, 2003)
37. R.W. Healy, T.C. Winter, J.W. Labaugh, O.L. Franke, *Water Budgets: Foundations for Effective Water-resources and Environmental Management* (U.S. Geological Survey Circular 1308, Reston, Virginia, 2007)
38. https://en.wikipedia.org/wiki/Atmosphere-of-Earth
39. S. Bashkin, J. Stoner, *Atomic Energy Levels and Grotrian Diagrams*, vol. 1–4 (Amsterdam, North Holland, 1975–1982)
40. J.P. Peixoto, A.H. Oort, *Physics of Climate* (American Institute of Physics, Washington, 1992)
41. K.E. Trenberth, L. Smith, T. Qian et al. J. Hydrometeorol. **8**, 758 (2007)
42. https://en.wikipedia.org/wiki/water-circle
43. https://water.usgs.gov/edu/watercycleatmosphere.html
44. https://en.wikipedia.org/wiki/Properties-of-water
45. *Handbook of Chemistry and Physics*, 86 edn, ed. D.R. Lide (London, CRC Press, 2003–2004)
46. P.C. Reist, *Introduction to Aerosol Science* (Macmillan Publishing Company, New York, 1984)
47. W.C. Hinds, *Aerosol Technology: Properties, Behavior and Measurement of Airborne Particles* (Wiley, New York, 1999)
48. R.F. Alder et al. J. Hydrometeor**4**, 147 (2003)
49. G.J. Huffman, R.F. Alser, D.T. Bolvin, G. Gu, Geoph. Res. Lett. **36**, L17808 (2009)
50. https://en.wikipedia.org/wiki/Electromagnetic-absorption-by-water
51. C.M.R. Platt, Quart. J. Roy. Meteorolog. Soc. **102**, 553 (2006)
52. J. Warner, Tellus **7**, 450 (1955)
53. B.J. Mason, *The Physics of Clouds* (Claredon Press, Oxford, 1971)

54. W.R. Leaitch, G.A. Isaak, Atmosp. Environ. **25**, 601 (1991)
55. https://en.wikipedia.org/wiki/Liquid-water-content
56. H. Svensmark, E. Frils-Christensen, J. Atmos. Terr. Phys. **59**, 1225 (1997)
57. H. Svensmark et al. Proc. Roy. Soc. **A463**, 385 (2007)
58. H. Svensmark, T. Bondo, J. Svensmark. Geophys. Res. Lett. **36**, L151001 (2009)
59. H. Svensmark, M.B. Enghoff, J.O.P. Pedersen, Phys. Lett. A **377**, 2343 (2013)